arXiv:cond-mat/0101248v1 [cond-mat.mes-hall] 16 Jan 2001

# Supercurrents through gated superconductor–normal-metal–superconductor contacts: the Josephson-transistor

Daniel D. Kuhn[a], Nikolai M. Chtchelkatchev[b], Gordey B. Lesovik[b], and Gianni Blatter[a]
[a] *Theoretische Physik, ETH-Hönggerberg, CH-8093 Zürich, Switzerland*
[b] *L. D. Landau Institute for Theoretical Physics, 117940 Moscow, Russia*
(February 1, 2008)

We analyze the transport through a narrow ballistic superconductor–normal-metal–superconductor Josephson contact with non-ideal transmission at the superconductor–normal-metal interfaces, e.g., due to insulating layers, effective mass steps, or band misfits (SIN interfaces). The electronic spectrum in the normal wire is determined through the combination of Andreev- and normal reflection at the SIN interfaces. Strong normal scattering at the SIN interfaces introduces electron- and hole-like resonances in the normal region which show up in the quasi-particle spectrum. These resonances have strong implications for the critical supercurrent $I_c$ which we find to be determined by the lowest quasi-particle level: tuning the potential $\mu_{x0}$ to the points where electron- and hole-like resonances cross, we find sharp peaks in $I_c$, resulting in a transitor effect. We compare the performance of this Resonant Josephson-Transistor (RJT) with that of a Superconducting Single Electron Transistor (SSET).

PACS numbers: 74.80.Fp, 74.50.+r, 74.60.Jg

## I. INTRODUCTION

The ability to control the supercurrent flow through narrow superconductor–normal-metal–superconductor (SNS) contacts is not only of scientific interest but also provides many opportunities for applications[1]. With recent progress in nanofabrication technology it has become possible to study devices in which electrons propagate ballistically and where the transport proceeds via few conduction channels[2]. Using gated SNS junctions[3], the transparency of the normal region can be manipulated: in a transparent wire, Andreev scattering at the NS boundaries produces phase-sensitive quasi-particle levels which carry large supercurrents; conversely, if the transmission is not ideal the admixture of normal scattering reduces the supercurrent transport. Accordingly, SNS junctions with a tunable transmission through the normal part define a natural setup for a superconducting transistor device[4–6].

Recent interest on transport through narrow channels and quantum point contacts concentrates on diverse phenomena such as conductance quantization in normal constrictions[2,7–10], supercurrent quantization in superconducting SNS junctions[3,8,11–13], or the transistor effect in super-links using either gated structures[4,6,14] or injection techniques[15–17]. Experimentally, such junctions are fabricated using superconductor—semiconductor-heterostructures[2,3,14,16], break-junctions[7–9], metal-nanolithography[15,17], or with the use of carbon nanotubes[18]. Theoretically, transport through normal constrictions has been studied by Glazman *et al.*[10,19] within a quasi-classical description assuming adiabatic joints between the channel and the leads. The corresponding extension to superconducting leads by means of a scattering matrix approach is due to Beenakker[11], see also Ref. 20, while Furusaki *et al.*[12] proceeded with the numerical analysis of junctions with non-adiabatic geometries and non-ideal interfaces. The evolution of the quasi-particle spectrum and the supercurrent quantization in a gated narrow SNS junction, as well as its transformation into a SIS tunnel junction, has been recently described by Chtchelkatchev *et al.*[13] Here, we extend this analysis to the study of SINIS junctions, where 'I' stands for a non-ideal interface between the superconducting banks S and the normal channel N.

In an ideal SNS junction the quasi-particle spectrum is determined by the Andreev-scattering[22] at the SN boundaries producing phase-sensitive levels transporting large supercurrents[13]. The position and relative arrangement of these states strongly depends on the chemical potential in the wire as well as on the phase difference between the superconducting banks. The inclusion of weak normal scattering at the SIN interface will only softly modify this quasi-particle spectrum through the mixing of (left- and right-) current carrying Andreev states. On the contrary, strong interface scattering introduces electron- and hole- like resonances within the normal region, defining a new starting point. The position of these resonances again depends on the wire's effective chemical potential. Tuning a pair of electron- and hole-like resonances to degeneracy these will be mixed by the Andreev-scattering and new phase sensitive levels are formed carrying supercurrent. This mechanism then provides a natural setup for the implementation of a superconducting Josephson field effect transistor[4,6] where the supercurrent is switched on and off by tuning the scattering resonances into degeneracy through the manipulation of a potential, e.g., through external gates. Model studies of such systems for individual resonances have been

carried out recently by Wendin and coworkers[6].

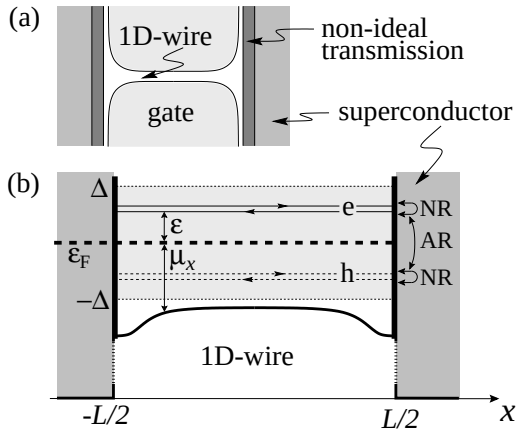


FIG. 1. Narrow channel SINIS contact with non-ideal interfaces, e.g., insulating layers, effective mass steps, or band misfits. We consider adiabatic constrictions to avoid the mixing of transverse channels. (a) Geometrical setup showing the gates narrowing the wire, (b) potential landscape with a flat barrier bounded by $\delta$-scatterers modelling insulating layers. All sources of non-ideal transmission account for *normal* reflections (NR), whereas the discontinuities of the gap parameter $\Delta$ are responsible for Andreev reflections (AR).

Below we proceed in two steps: After a brief definition of the problem (Sec. II), we first determine the scattering states of the corresponding problem where the superconducting banks are replaced by normal-metallic leads, the NININ junction. Second, we reinstall the superconducting banks and determine the mixing of the (electron- and hole-like) normal scattering states through Andreev-scattering at the normal-superconductor interface. In Sec. III we analyze the quasi-particle spectrum for weak and strong normal scattering at the NIS interfaces. Section IV is devoted to the calculation of the supercurrent; we discuss the functionality of the Resonant Josephson Transitor (RJT) and compare this device with the Superconducting Single Electron Transistor (SSET).

## II. BALLISTIC CONTACTS: SCATTERING MATRIX APPROACH

We consider a narrow metallic lead with few transverse channels connecting two superconducting banks with a rectangular pair potential $\hat{\Delta}(x<-L/2)=\Delta\exp(i\varphi_{\rm L})$, $\hat{\Delta}(|x|<L/2)=0$ and $\hat{\Delta}(x>L/2)=\Delta\exp(i\varphi_{\rm R})$, see Fig. 1(a). Joining the channel adiabatically to the superconducting banks, the transverse channels in the wire are separable[19] and for each of them the quasi-particle spectrum $\varepsilon_\nu$ is determined through the 1D Bogoliubov-de Gennes equation (we choose states with $\varepsilon_\nu\geq 0$)

$$\begin{bmatrix}\mathcal{H}_0 & \hat{\Delta}(x)\\ \hat{\Delta}^*(x) & -\mathcal{H}_0\end{bmatrix}\begin{bmatrix}u_\nu(x)\\ v_\nu(x)\end{bmatrix}=\varepsilon_\nu\begin{bmatrix}u_\nu(x)\\ v_\nu(x)\end{bmatrix}, \qquad (1)$$

with $\mathcal{H}_0=-\hbar^2\partial_x[1/2m(x)]\partial_x+U(x)-\mu_x(x)$ and where $u_\nu$ and $v_\nu$ denote the electron- and hole-like components of the wave function $\Psi_\nu$. The potential $U(x)$ induces normal scattering at the NS interface and is due to an insulating layer or a band offset, for example. Similarly, the mass $m(x)$ may change at the NS interface, again generating normal scattering. The transverse energy $\varepsilon_\perp(x)$ of the channel is enclosed in the effective chemical potential[19] $\mu_x(x)=\varepsilon_{\rm F}-\varepsilon_\perp(x)$. We will also make use of the kinetic energies $E=\varepsilon_{\rm F}\pm\varepsilon$ of electron (+) and hole (−) states as measured with respect to the band bottom in the superconductors.

The spectrum splits into continuous and discrete contributions and we will concentrate on the latter part with $\varepsilon_\nu<\Delta$ in the following, as it provides the main contribution to the critical supercurrent in the most interesting transport regimes, see below. We solve the Bogoliubov-de Gennes equation for the SINIS junction with the help of the usual transfer-matrix technique[24]. In order to do so we first have to determine the resonance structure of the related NININ problem that arises if we replace the superconductors by normal metallic leads.

### A. NININ-junctions

We expand the scattering states in a basis of in- and outgoing states $\Psi^{\rm in,out}_{\rm R,L}$ on both sides of the wire, with phases that vanish at the interfaces[25] $\pm L/2$,

$$\Psi_{\rm L}(x)=a^{\rm in}_{\rm L}e^{ik(x+L/2)}+a^{\rm out}_{\rm L}e^{-ik(x+L/2)}, \qquad (2)$$
$$\Psi_{\rm R}(x)=a^{\rm in}_{\rm R}e^{-ik(x-L/2)}+a^{\rm out}_{\rm R}e^{ik(x-L/2)}, \qquad (3)$$

with $k(E)=\sqrt{2mE}/\hbar$ the wave vector of an incident particle. The energy dependent scattering matrix $\mathcal{S}$ connects the expansion coefficients $a^{\rm in,out}_{\rm R,L}$ (here, $t$ and $r$ denote the moduli of the matrix elements),

$$\begin{bmatrix}a^{\rm out}_{\rm R}\\ a^{\rm out}_{\rm L}\end{bmatrix}=\begin{bmatrix}t\exp(i\chi^t) & -r\exp(i[2\chi^t-\chi^r])\\ r\exp(i\chi^r) & t\exp(i\chi^t)\end{bmatrix}\begin{bmatrix}a^{\rm in}_{\rm L}\\ a^{\rm in}_{\rm R}\end{bmatrix}; \qquad (4)$$

with this definition of the $\mathcal{S}$-matrix and the basis states, the scattering phases account for the propagation through the wire. E.g., for a vanishing transverse energy in the normal region and in the absence of any interface barrier a finite phase $\chi^t=kL$ is picked up.

We describe the effective chemical potential in the normal region through a smooth function characterized by its minimum $\mu_x(0)=\mu_{x0}$ and a positive curvature $m\Omega^2=\partial_x^2\mu_x$ (see Fig. 1(b)). The parameter $\mu_{x0}$ (i.e., the diameter of the metallic wire) is assumed to be tunable by means of external electrostatic gates. In a long wire the potential is flat, $\hbar\Omega\ll\Delta$, and produces a sharp switching between transmission and reflection within the energy interval $\hbar\Omega$; the corresponding transverse energy $\varepsilon_\perp(x)$ defines a smooth and flat potential barrier in the interval $(-L/2,L/2)$. In the following we refer to such

barriers as *smooth* and $t_i \exp(i\chi^{t_i})$ and $r_i \exp(i\chi^{r_i})$ denote the associated 'inner' scattering amplitudes describing the motion of the quasi-particles between $-L/2+0$ and $L/2-0$ (we use an analoguous definition of the 'inner' scattering amplitudes as in (4)). The particular smooth geometry of such inner barriers justifies the application of the Kemble formula[10] for the transmission probability, $t_i^2 = 1/\{1+\exp[-2\pi(\mu_x(0)\pm\varepsilon)/\hbar\Omega]\}$, whereas the quasi-classic method can be used to determine the scattering phases $\chi^{t_i}$ and $\chi^{r_i}$.

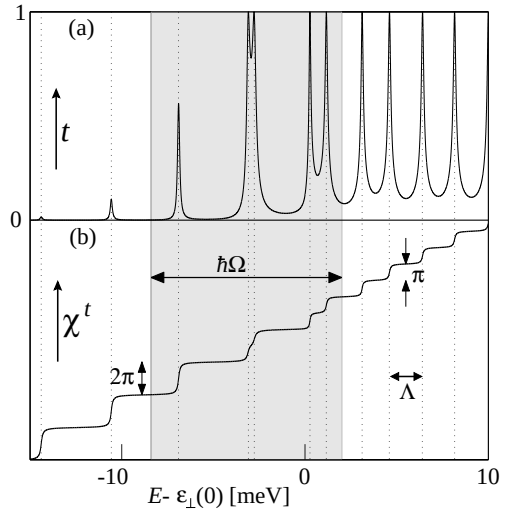


FIG. 2. Modulus and phase of the transmission amplitude through a parabolic barrier with $\delta$-scatterers at the edges (parameters: $Z=2$, $\varepsilon_\perp(0)=5$ eV, $L=2500$ nm). Note that the energy $E$ is swept and $\varepsilon_\perp(0)$ is kept fixed. A similar resonance structure is found for other sources of non-ideal transmission at $\pm L/2$.

In order to obtain the global scattering amplitudes $t\exp(i\chi^t)$ and $r\exp(i\chi^r)$ of the junction we have to include effects of normal scattering at the boundaries. As a typical example we consider symmetric smooth barriers of height $\varepsilon_{\rm F}-\mu_{x0}$ bounded by Dirac scatterers of strength $V_0$ at the interfaces (such a setup describes an NININ junction with insulating layers at the interfaces; see the Appendix for a brief discussion of other typical cases).

First, we concentrate on the global *transmission* amplitude $t\exp(i\chi^t)$ which is easily expressed in terms of the scattering amplitudes of the inner barrier and the Dirac $\delta$-scatterers, see the Appendix for details of the calculation. The main effect of the scattering at the channel boundaries is to introduce resonances at energies $E_{\rm res}$ which we call *perfect* (*imperfect*) if $t(E_{\rm res})=1$ ($<1$). For energies $E>\varepsilon_\perp(0)+\hbar\Omega/2$ the electrons easily propagate through the channel, while the reflection at the boundaries produces almost equidistant resonances with a spacing $\Lambda\approx\pi/\partial_E\chi^{t_i}\sim 2(\mu_{x0}\varepsilon_{\rm L})^{1/2}$, with $\varepsilon_{\rm L}=\hbar^2\pi^2/2mL^2$ (see Fig. 2; the last relation describes the case of a flat inner barrier). On the contrary, for small energies below $\varepsilon_\perp(0)-\hbar\Omega/2$, tunneling suppresses the propagation through the channel and only imperfect resonances separated by $\sim 2\Lambda$ survive. In the intermediate region, pairs of perfect resonances collapse and become imperfect. Moreover, the scattering phase $\chi^t$ grows with the energy and picks up a phase of $\pi$ and $2\pi$ at perfect and imperfect resonances, respectively. We refer to resonances at energies $E_{\rm res}=\varepsilon_{\rm F}+\hat{\varepsilon}_{\rm res}$ above $\varepsilon_{\rm F}$ as *electronic* and to those below, at $E_{\rm res}=\varepsilon_{\rm F}-\check{\varepsilon}_{\rm res}$, as *hole-like* resonances. Below, we will be mostly concentrating on the propagating regime with $E>\varepsilon_\perp(0)+\hbar\Omega/2$. In this regime the global transmission amplitude takes the form ($t_{i\pm}\approx 1$)

$$t\exp(i\chi^t)=\frac{e^{i\chi^{t_i}}}{1-Z^2+i2Z+Z^2e^{i2\chi^{t_i}}}, \qquad (5)$$

with $Z=mV_0/\hbar^2k_{\rm F}$ the dimensionless parameter giving the strength of the scattering potential. Resonances of width

$$\Gamma=\frac{2}{\partial_E\chi^t}=\frac{2\Lambda}{\pi}\frac{T}{2-T} \qquad \text{with} \qquad \Lambda=\frac{\pi}{\partial_E\chi^{t_i}} \qquad (6)$$

and a transmission probability $T=1/(1+Z^2)$ appear as the denominator in (5) touches the complex unit circle (note that $\Gamma\longrightarrow 2\hbar v/L$, with $v$ the particle velocity, in the absence of any scattering potential).

For symmetric barriers the *reflection* amplitude $r\exp(i\chi^r)$ is determined (up to $\pm1$) by the unitarity of the scattering matrix, i.e., $r=(1-t^2)^{1/2}$ and $\chi^r=\chi^t+\pi(n+1/2)$. The integer $n$ jumps by unity at perfect resonances.

### B. SINIS-junctions

After evaluating the normal scattering amplitudes we can reinstall the superconductors and match the scattering states in the normal region with the evanescent modes in the superconducting banks. We make use of the Andreev approximation[22] and obtain the quantization condition[11,13,23]

$$\cos(\chi_+^t-\chi_-^t-\alpha)=r_+r_-\cos\beta+t_+t_-\cos\varphi, \qquad (7)$$

where the $+(-)$ signs refer to the kinetic energies $\varepsilon_{\rm F}\pm\varepsilon$ of the electron(hole)-like states[26]. The Andreev scattering at the NS boundaries introduces the phase $\alpha=2\arccos(\varepsilon/\Delta)$ decreasing from $\pi$ at $\varepsilon=0$ to 0 at the gap $\varepsilon=\Delta$, as well as the phase difference $\varphi=\varphi_{\rm L}-\varphi_{\rm R}$ between the two superconducting banks. For symmetric barriers the phase $\beta=(\chi_+^t-\chi_+^r)-(\chi_-^t-\chi_-^r)$ is a multiple of $\pi$ and produces a smooth function $r_+r_-\cos\beta$ changing sign at perfect resonances [see Fig. 5(b)].

The case of an ideal SNS junction where the effective chemical potential joins smoothly to the band bottom in the superconductors has been analyzed by Chtchelkatchev *et al.*[13] In this special situation the global

and inner scattering amplitudes coincide and resonances are absent. Sweeping $\mu_{x0}$, they find a one parametric ($\mu_{x0}$) family of discrete spectra describing the transition of an insulating SIS tunnel junction (at $\mu_{x0} \ll -\Delta$) into a ballistic SNS structure (at $\mu_{x0} \gg \Delta$), see Fig. 3(a). More precisely, electronic levels with an exponentially small dependence on the phase $\varphi$ are converted into phase sensitive Andreev-levels as $\mu_{x0}$ is increased, i.e., as the band bottom in the wire is lowered. It turns out that the critical supercurrent is carried by the lowest state, $I_c = \max_\varphi[(2e/\hbar)\partial_\varphi \varepsilon_0]$, and is realized for a phase $\varphi = \pi - 0$. Increasing the channel width, the critical supercurrent increases in steps of $e/(\tau_0 + \hbar/\Delta)$ as new transverse channels open. The travel time $\tau_0$ of the quasi-particles is easily calculated within the quasiclassical scheme and approaches the asymptotic value $\tau_0 \sim L/v_{\mathrm{F},x}$ in the open channel. This analysis explains the dependence of the non-universal critical supercurrent steps on the junction parameters.

In the following we go beyond the analysis of Chtchelkatchev *et al.* and determine the spectrum and the supercurrent transport in a narrow ballistic SINIS Josephson junction including resonant barriers in the normal region, see Fig. 1(b).

## III. QUASI-PARTICLE SPECTRUM

Below we shall see that the bound state spectrum of junctions with smooth barriers is only slightly modified by switching on weak resonances, see Fig. 3(b), with the degeneracy of the Andreev levels at $\varphi = 0$ and $\pi$ lifted. For a fixed pair of levels $\varepsilon^{(\pm)}$, this splitting $\delta\varepsilon = \varepsilon^{(+)} - \varepsilon^{(-)}$ is roughly a periodic function of $\mu_{x0}$ with a period $\Lambda$ reflecting the resonance spacing. As the strength of the interface scattering increases the discrete spectrum is gradually distorted (see Fig. 3(c)); the phase sensitivity at large chemical potential $\mu_{x0}$ (region I) is reduced and the bound state energies align with the resonance energies of the normal NININ setup. The effect of interface scattering on the continuum part of the spectrum has been analyzed in Ref. 23.

### A. Weak Resonances

We first concentrate on weak resonances characterized by a small scattering parameter $Z \ll 1$. In particular, we aim at estimating the level splitting in the Andreev spectrum shown in Fig. 3(b). Using Eq. (5) we evaluate the terms on the right side of the quantization condition (7) to lowest order in $Z$ and find $t_+t_- = 1 - 2Z^2[\cos^2\chi_+^{t_i} + \cos^2\chi_-^{t_i}]$ and $r_+r_- = 4Z^2|\cos\chi_+^{t_i}||\cos\chi_-^{t_i}|$. For symmetric barriers and as a consequence of the unitarity of the scattering matrix, the rescaled phase $\beta(\varepsilon)/\pi$ is an integer valued function starting from 0 at $\varepsilon = 0$ and jumping by unity whenever $\varepsilon$ lines up with a (perfect) resonance at $\hat{\varepsilon}_{\mathrm{res}}$ or $\check{\varepsilon}_{\mathrm{res}}$ of the junction. We then may write $\cos\beta = (-1)^n$, where $n(\varepsilon)$ denotes the number of perfect resonances within the interval $(0, \varepsilon)$. Hence, $\cos\beta$ generates a smooth contribution $r_+r_-\cos\beta = 4Z^2\cos\chi_+^{t_i}\cos\chi_-^{t_i}$, which is small, of order $Z^2$. Finally, the scattering phase $\delta\chi^t = \chi_+^t - \chi_-^t$ in (7) may be identified with $\delta\chi^{t_i} = \chi_+^{t_i} - \chi_-^{t_i}$; the deviation of $\delta\chi^t$ from $\delta\chi^{t_i}$ provides only small corrections of order $Z^2$ to the splitting in the Andreev spectrum and thus can be disregarded.

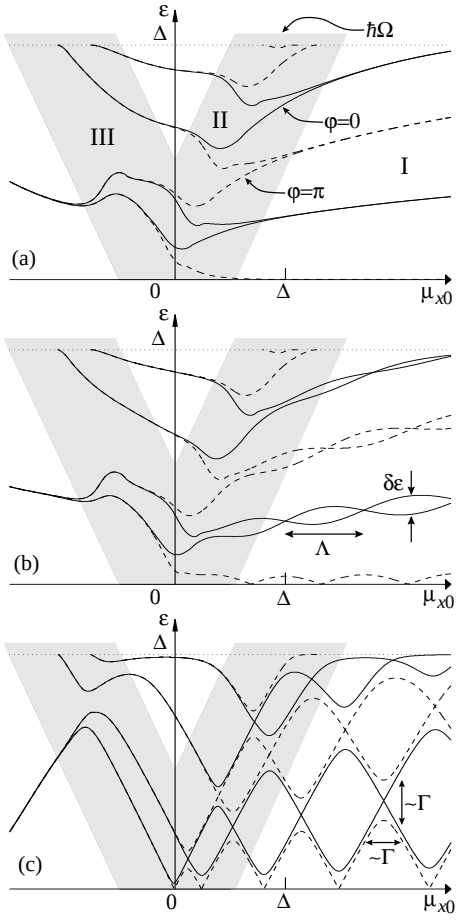


FIG. 3. Discrete energy spectrum for a smooth parabolic potential barrier bounded by Dirac scatterers of strength $V_0$ ($Z = mV_0/\hbar^2 k_{\mathrm{F}}$; parameters are chosen to emphasize the overall structure of the spectrum). In regions I and II the quasi-particle energies depend on the phase $\varphi$ ($\varphi = 0$: solid lines, $\varphi = \pi$: dashed lines). Note that the degeneracies in region I are lifted for $\varphi \neq 0, \pm\pi$. (a) The unperturbed spectrum for $Z = 0$ as discussed by Chthelkatchev *et al.*[13] (b) At $Z = 0.1$ the junction exhibits weak resonances which lead to a splitting in the Andreev spectrum; the period $\Lambda$ reflects the resonance spacing. (c) For $Z = 1$ the junction develops distinct resonances to which the quasi-particle levels are pinned. The remaining degeneracies are a consequence of the almost identical resonance shapes.

At $\varphi = 0$ the right hand side of (7) can be expressed as $R = 1 - 2Z^2(1 - \cos\delta\chi^{t_i})(1 - \cos\Sigma\chi^{t_i})$ while the left hand side takes the form $L = \cos(\delta\chi^{t_i} - \alpha)$. The sum $\Sigma\chi^{t_i} = \chi_+^{t_i} + \chi_-^{t_i}$ of the scattering phases depends only weakly on $\varepsilon$ but increases linearly in $\mu_{x0}$ with a slope $2\pi/\Lambda$, as follows from linearizing $\chi_\pm^{t_i}(\varepsilon, \mu_{x0})$. On the other hand, the phase difference $\delta\chi^{t_i}$ increases with energy $\varepsilon$ but is roughly independent of $\mu_{x0}$. Both terms $L$ and $R$ then show an oscillating dependence on $\delta\chi^{t_i}$ and on the energy $\varepsilon$ (see Fig. 4), while their relative phase $\alpha(\varepsilon)$ slowly decreases from $\pi$ at $\varepsilon = 0$ to 0 at $\varepsilon = \Delta$. Thus, for small energies ($\varepsilon \ll \Delta$) the maxima in $L$ coincide with the minima in $R$ and we obtain a large splitting,

$$\delta\varepsilon \approx \frac{4}{\pi} Z\Lambda |\sin\chi_+^{t_i}|, \tag{8}$$

to lowest order in $Z$ (with $\chi_+^{t_i}$ evaluated at $\varepsilon = 0$). The corresponding splitting for $\varphi = \pm\pi$ is proportional to $|\cos\chi_+^{t_i}|$ with the same prefactor. With increasing energy the phases of $L$ and $R$ match up and the splitting becomes small, see Fig. 4. The monotonous decrease of the splitting is most prominent in long junctions with many trapped levels.

As manifested in (8) the splitting vanishes at specific degeneracy points: we define the $(l, m)$-degeneracy via the condition $\varepsilon_{\rm F} = (E_{\rm res}^l + E_{\rm res}^m)/2$, where $l$ and $m$ count the perfect resonances. This implies $|E_{\rm res}^l - E_{\rm res}^m|/2 = \hat{\varepsilon}_{\rm res} = \check{\varepsilon}_{\rm res} = \varepsilon_{\rm res}^{\rm d}$. The ideal degeneracies in (8) originate from the assumption that all perfect resonances have the same symmetric shape, $t(E_{\rm res}^l + \delta E) = t(E_{\rm res}^m \pm \delta E)$. For $\varphi = 0$ ($\pm\pi$) and for even (odd) values of $n(\varepsilon_{\rm res}^{\rm d})$ the right hand side of the quantization condition (multiplied by $-1$) equals unity, $r_+r_- + t_+t_- = r_+^2 + t_+^2 = 1$, and thus the trapped levels appear in degenerate pairs. The degeneracy is lifted, if we take into account that the perfect resonances are not identical.

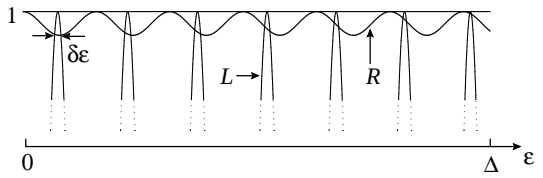


FIG. 4. The quasi-particle energies are determined by the intersections of the right and the left hand side ($R$ and $L$) of the quantization condition (7). Every maximum in $L$ contributes a pair of trapped levels split by $\delta\varepsilon$.

### B. Strong Resonances

Let us next study the effects of *strong* resonances. Without loss of generality we again discuss the symmetric barrier bounded by $\delta$-scatterers (see also Ref. 23) . We concentrate on the open channels in region I (see Fig. 3(a)); the other regimes in the $(\varepsilon, \mu_{x0})$-plane are less interesting and we will briefly discuss them at the end. For sharp resonances with $\Gamma \ll \Delta$ the transmittivity close to a resonance $\varepsilon_{\rm res}$ assumes a Lorentz profile[27] $t_\pm(\varepsilon) = (\Gamma/2)/\sqrt{(\varepsilon - \varepsilon_{\rm res})^2 + (\Gamma/2)^2}$ and the scattering phase takes the usual form $\chi_\pm^t(\varepsilon) = \chi^t(E_{\rm res}) \pm \arctan[2(\varepsilon - \varepsilon_{\rm res})/\Gamma]$.

Fig. 5 shows the terms entering the quantization condition (7). Particles incident from the left on the normal region are reflected back ($r_+ \approx 1$) unless their energy coincides with an electronic resonance energy ($r_+(\hat{\varepsilon}_{\rm res}) = 0$ for perfect resonances). Similarly, holes are only transmitted if their energy corresponds to a hole-like resonance energy ($r_-(\check{\varepsilon}_{\rm res}) = 0$). Consequently, the product $r_+r_-$ remains close to unity but sharply drops to zero at perfect resonance energies (see Fig. 5(a)). Similar to the case of weak resonances the product $r_+r_-$ becomes a smooth function of $\varepsilon$ when combined with $\cos\beta = (-1)^n$, see Fig. 5(b). Furthermore, the phase sensitive term $t_+t_-\cos\varphi$ vanishes practically over the entire interval $[0, \Delta]$ (see Fig. 5(c)) with the exception of specific points where particle- and hole- resonances become *degenerate*, $\hat{\varepsilon}_{\rm res} = \check{\varepsilon}_{\rm res} = \varepsilon_{\rm res}^{\rm d}$.

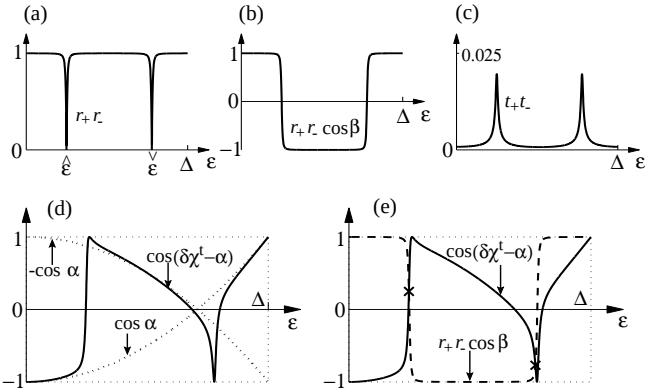


FIG. 5. The various terms entering the quantization condition (7) in the limit $\Gamma \ll \Delta$: We show the case of perfect *isolated* resonances ($|\hat{\varepsilon} - \check{\varepsilon}| \gg \Gamma$), where the product $t_+t_-$ is small at all energies (here, $t_+t_- < 0.025$). The bound state energies (marked with crosses in (e)) are determined by the intersections of $\cos(\delta\chi^t - \alpha)$ and $r_+r_-\cos\beta$.

The left hand side of (7) is mainly determined by the phase difference $\delta\chi^t$ exhibiting sharp steps by $\pi$ at the resonance energies $\check{\varepsilon}_{\rm res}$ and $\hat{\varepsilon}_{\rm res}$ while remaining constant in between (in our discussion of the situation away from region I below, we will have to distinguish perfect from imperfect resonances, as the latter involve phase jumps by $2\pi$). Hence, in the limit $\Gamma \to 0$ we obtain $\cos(\delta\chi^t - \alpha) = (-1)^n\cos\alpha$ while a small finite value of $\Gamma$ will smooth the discontinuities (see Fig. 5(d)). All the terms entering the quantization condition (7) then are pronounced functions of $\varepsilon$ near the resonance energies while staying roughly constant everywhere else. As a consequence, the intersections of the left and the right hand side of (7) come to lie close to the resonance en-

ergies of the NININ-junction as shown in Fig. 5(e) and we conclude that the normal state resonances attract the quasi-particle bound states, $\varepsilon \approx \varepsilon_{\rm res}$ to zeroth order in $\Gamma$. The predicate *electronic-* and *hole-like* states then can be naturally assigned to the trapped levels in the SINIS junction, too.

In region I (see Fig. 3(a)), the bound state energy close to an *isolated resonance* is determined by the implicit equation

$$\varepsilon = \varepsilon_{\rm res} - \frac{\Gamma}{2}\cot[\alpha(\varepsilon)/2]. \qquad (9)$$

This equation follows directly from the quantization condition (7) with $t_+\exp(i\chi_+^t)$ described by an ideal Lorentzian resonance while $t_- = 0$, $r_- = 1$, and $\chi_-^t = \chi_+^t(\varepsilon_{\rm res}) + n(\varepsilon_{\rm res})\pi$ is constant (or vice versa $+ \leftrightarrow -$). For $\varepsilon \ll \Delta$ we may approximate $\alpha(\varepsilon) \approx \pi$, while at $\varepsilon \lesssim \Delta$ (9) is easily analyzed graphically (note, however, that the above assumptions for $t_\pm$ and $\chi_\pm^t$ are only valid if $|\varepsilon - \varepsilon_{\rm res}| \ll \Delta$). The phase independence of the quasi-particle states in the presence of strong normal scattering is made explicit in the result (9).

Close to the *particle-hole degenerate resonances* the phase sensitive term $t_+t_- = (\Gamma/2)^2/[(\varepsilon-\varepsilon_{\rm res}^{\rm d})^2 + (\Gamma/2)^2]$ is of order unity and we obtain pairs of trapped levels

$$\varepsilon^{(\pm)} = \begin{cases} \varepsilon_{\rm res}^{\rm d} - \frac{\Gamma}{2}\left(\cot(\frac{\alpha}{2}) \pm \frac{|\sin(\varphi/2)|}{\sin(\alpha/2)}\right), & n(\varepsilon_{\rm res}^{\rm d}) \text{ even}, \\ \varepsilon_{\rm res}^{\rm d} - \frac{\Gamma}{2}\left(\cot(\frac{\alpha}{2}) \pm \frac{|\cos(\varphi/2)|}{\sin(\alpha/2)}\right), & n(\varepsilon_{\rm res}^{\rm d}) \text{ odd} \end{cases} \qquad (10)$$

(we assume both scattering amplitudes $t_\pm\exp(i\chi_\pm^t)$ to be described by the same Lorentzian centered around $\varepsilon_{\rm res}^{\rm d}$; Eq. 10 agrees with the result of Ref. 6 obtained for a short junction[27], see also Ref. 23). The levels (10) are manifestly phase sensitive and become degenerate at $\varphi = 0$ for even $n$ and at $\varphi = \pi$ if $n$ is odd. For low energies $\varepsilon \ll \Delta$ we estimate $\alpha(\varepsilon) \approx \pi$ and the maximum level splitting is $\delta\varepsilon \approx \Gamma$. We conclude that phase sensitivity survives only in a narrow interval of order $\Delta\mu_{x0} \sim \Gamma$ around the degeneracy points $\mu_{x0}^{\rm d}$, being negligible everywhere else (see Fig. 3(c)).

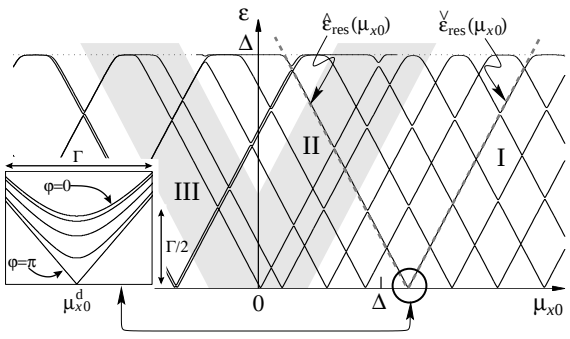


FIG. 6. Discrete spectrum for a triple barrier generating narrow resonances (from a numerical solution of the quantization condition (7)). The levels are pinned to the resonances; note that hole-like resonance energies $\check{\varepsilon}_{\rm res}$ grow with $\mu_{x0}$ whereas electronic resonance energies $\hat{\varepsilon}_{\rm res}$ decrease. In region II (III) the hole-like (electronic) levels pair up such that the branches of imperfect resonances carry two bound states. The inset shows the lowest level near the degeneracy point $\mu_{x0}^{\rm d}$ for different values of $\varphi$ ($\varphi = j\pi/4$, $j = 0\ldots4$).

Above we have found the trapped levels belonging to a branch $\varepsilon_{\rm res}(\mu_{x0})$ of perfect resonances at the degeneracy points $\mu_{x0}^{\rm d}$ and far away, $|\mu_{x0} - \mu_{x0}^{\rm d}| \gg \Gamma$. In between we can interpolate (9) and (10) by means of the usual hyperbolic dispersion relation and obtain (in the limit $\varepsilon \ll \Delta$; $\alpha \approx \pi$)

$$\varepsilon^{(\pm)}(\mu_{x0}) = \varepsilon_{\rm res}^{\rm d} \pm \sqrt{(\mu_{x0} - \mu_{x0}^{\rm d})^2 + [\Gamma\cos(\varphi/2)/2]^2}, \quad (11)$$

where we have assumed that $n(\varepsilon_{\rm res}^{\rm d})$ is odd and $\partial_{\mu_{x0}}\check{\varepsilon}_{\rm res} \approx -\partial_{\mu_{x0}}\hat{\varepsilon}_{\rm res} \approx 1$. The result (11) will be useful in our discussion of the transport properties below.

In region II (see Fig. 3(a)) the perfect hole-like resonances pair up and collapse as $\mu_{x0}$ is lowered, thus generating imperfect resonances, see Fig. 6. The analogous collapse of the electronic resonances is shifted to region III. Note that an imperfect resonance carries *two* nearly degenerate levels guaranteeing that the number of bound states remains conserved upon changing $\mu_{x0}$.

### C. Other Sources of Non-ideal Transmission

The above analysis has been based on $\delta$-scatterers modelling the effects of an insulating layer in an SIN interface. Assuming other sources of non-ideal transmission at $\pm L/2$ we have to modify some of the above results: In order to describe junctions with potential steps $V_{\rm S}$ at the edges we introduce the wave vector $k_{\rm nw} = \sqrt{2m(E - V_{\rm S})}/\hbar$ in the normal wire and distinguish it from the analogous quantity $k_{\rm sc} = \sqrt{2mE}/\hbar$ in the superconductor. With $\kappa \equiv (k_{\rm sc}/k_{\rm nw} + k_{\rm nw}/k_{\rm sc})/2 \geq 1$ the transmission probability takes the form $T = 2/(1+\kappa)$ (see the Appendix). In the presence of weak resonances ($T \lesssim 1$), Eq. (8) for the gaps in the Andreev spectrum reads $\delta\varepsilon \approx 4\Lambda\sqrt{1-T}\,|\cos\chi^{t_i}|/\pi$, while the results for strong resonances remain the same (see (9)). A step in the effective mass at the interface produces a similar result: with $m(|x| > L/2) = m_{\rm sc}$ and $m(|x| < L/2) = m_{\rm nw}$ the ratio of wave vectors entering the parameter $\kappa$ takes the form $k_{\rm sc}/k_{\rm nw} = \sqrt{m_{\rm sc}/m_{\rm nw}}$. Finally, combining all three effects, a potential step, an effective mass discontinuity, and an insulating layer (in the form of a $\delta$-function scatterer) at the interface, the transmission probability can be written in the form

$$T = \frac{4k_{\rm sc}k_{\rm nw}m_{\rm sc}m_{\rm nw}}{(k_{\rm nw}m_{\rm sc} + k_{\rm sc}m_{\rm nw})^2 + 4V_0^2m_{\rm sc}^2m_{\rm nw}^2/\hbar^4}; \qquad (12)$$

obviously, the various scattering mechanisms are non-additive and Matthiessen's rule is not applicable.

Slightly asymmetric junctions have essentially the same properties as the idealized symmetric ones. An NINI'N junction with insulating layers of different transparency, $T_{\min} \lesssim T_{\max}$, exhibits large imperfect resonances[24] of height $t^2(E_{\rm res}) \approx T_{\min}/T_{\max}$ instead of perfect resonances with unit transmission. Furthermore, $\chi^r$ is now a continuous function of energy; the discontinuous jumps by $\pi$ are smeared (with $\chi^r$ increasing monotonuously for $T_{-L/2} < T_{L/2}$ and bounded for the opposite case with $T_{L/2} < T_{-L/2}$; note that $\chi^r + \chi^{r'} = \pi + 2\chi^t$, $\chi^{r'}$ the corresponding phase for a particle incident from the left) and $\cos\beta$ changes rapidly but smoothly between $\pm 1$ at the resonance energies. Since all terms entering the quantization condition (7) are only weakly affected by small asymmetries, the above discussion of the electronic properties remains valid for (weakly) non-symmetric junctions.

## IV. TRANSPORT

We proceed with the investigation of the transport properties of the symmetric SINIS junctions in region I (see Fig. 6) and concentrate on the situation characterized by strong resonances with $\Gamma/\Lambda \ll 1$. Given the dependence of the quasi-particle energy $\varepsilon$ on the phase $\varphi$, the contribution of the level to the supercurrent follows from a simple derivative, $I = (2e/\hbar)\partial_\varphi \varepsilon$ (a factor 2 has been included to account for spin-degeneracy).

### A. Generic case

We first consider the generic case where a level is pinned to an isolated (electronic) resonance. In this situation we can assume $t_+ \sim 1$, $t_- \propto \Gamma/\Lambda$ and $\cos(\delta\chi^t - \alpha) - r_+ r_- \cos\beta \propto \varepsilon/\Gamma + \text{const.}$ (see also Fig. 5). Within this approximation $t_+ t_- \propto \Gamma/\Lambda$ is small and linearly related to $\delta\varepsilon = \max_\varphi[\varepsilon(\varphi)] - \min_\varphi[\varepsilon(\varphi)]$ through the large slope $1/\Gamma$. We then estimate $\delta\varepsilon \propto \partial_\varphi \varepsilon \propto \Gamma^2$ and find that each level contributes a small supercurrent, of order $\Gamma^2$.

### B. Degenerate resonances

The phase sensitivity of the trapped levels is dramatically increased close to degenerate resonances, see Eq. (11). However, still assuming narrow resonances with $\Gamma/\Lambda \ll 1$, the supercurrent in general remains small: within our approximation the contributions arising from a pair of nearly degenerate levels cancel each other due to the symmetry $\partial_\varphi \varepsilon^{(+)} = -\partial_\varphi \varepsilon^{(-)}$ (a more accurate analysis provides a residual contribution of order $\Gamma^2$, see[28]). Furthermore, the continuous part of the spectrum again contributes with a term of order $\Gamma^2$. The only situation producing a large current (of order $\Gamma$) then is realized at the special degeneracy points produced by an (electronic) resonance crossing the Fermi level, where $\hat{\varepsilon}_{\rm res}(\mu^{\rm d}_{x0}) \approx \check{\varepsilon}_{\rm res}(\mu^{\rm d}_{x0}) \approx 0$, see Fig. 6. With its energy $\varepsilon_0^{(+)}$ described by (11), this level carries a nonvanishing supercurrent of magnitude

$$I_0 = \frac{2e}{\hbar}\frac{\Gamma^2}{16}\frac{\sin\varphi}{\sqrt{(\mu_{x0}-\mu^{\rm d}_{x0})^2 + (\Gamma/2)^2\cos^2(\varphi/2)}}. \qquad (13)$$

With one channel open, we then find that a large critical supercurrent

$$I_{\rm c}(\mu_{x0}) = \frac{e\Gamma}{2\hbar}\left[\sqrt{1+\left[\frac{(\mu_{x0}-\mu^{\rm d}_{x0})}{\Gamma/2}\right]^2} - \frac{|\mu_{x0}-\mu^{\rm d}_{x0}|}{\Gamma/2}\right] \qquad (14)$$

is realized near the special values $\mu^{\rm d}_{x0}$ for the chemical potential where $\varepsilon^{\rm d}_{\rm res}(\mu^{\rm d}_{x0}) = 0$ and for $\varphi = \pi - 0$. This large supercurrent flow quickly vanishes as $\mu_{x0}$ is tuned away from these degeneracy points by an energy larger than the resonance width $\Gamma$, see Fig. 7. Below, we refer to such a tunable SINIS junction as a *Resonant Josephson-Transistor* (RJT) (alternative schemes leading to a transistor effect make use of resonant electromagnetic pumping[29] or injection of quasi-particles into specific levels via multiprobe devices, see Refs. 28,30,15–17). Note that the chemical potential $\mu_{x0}$ is not directly accessible but only through the gate voltage $V_{\rm g}$, thus introducing the slope $d\mu_{x0}/dV_{\rm g}$ as an additional characteristic parameter of the device. Also, we point out that a sharp transistor effect requires the temperature to be low, $k_{\rm B}T < \Gamma$.

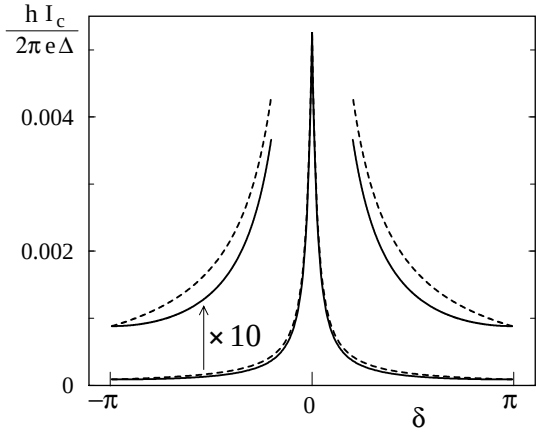


FIG. 7. Critical current versus chemical potential $\mu_{x0} = \delta\hbar/2\tau|_{\varepsilon_{\rm F}}$ for a sharp resonance with $T = 0.1$ and $\tau|_{\varepsilon_{\rm F}} = 10\hbar/\Delta$. The approximation (14) (dashed line) agrees with the exact result obtained via the Green's function analysis at resonance and midway between resonances, $\delta = 0, \pm\pi$, and provides a good estimate in between.

The result (14) appears to be valid in the immediate vicinity of a resonance crossing the Fermi level. However, comparing this result with the one derived from a full Green's function analysis[31] of the long ($L \gg \xi$) SINIS junction with sharp resonances ($\Gamma/\Lambda \ll 1$) one finds that the result (14) is exact at the degeneracy points $\mu_{x0} \approx \mu_{x0}^{\rm d}$ and, as it turns out, also midway in between two such degeneracies; defining the parameter $\delta = 2S|_{\varepsilon_{\rm F}}/\hbar \approx 2(\mu_{x0} - \mu_{x0}^{\rm d})\tau|_{\varepsilon_{\rm F}}/\hbar + 2n\pi$ the result (14) then is exact at all multiples of $\pi$, $\delta \approx n\pi$ (here, $S|_{\varepsilon_{\rm F}}$ denotes the action for an electron traversing the normal region $[-L/2+0, L/2-0]$ at the Fermi level and $\tau \equiv \partial_\varepsilon S$ is the travel time). Furthermore, in between the points $\delta = n\pi$ the deviations of (14) from the exact Green's function result are small, see Fig. 7.

### C. Josephson- versus Single Electron Transistor

Next we discuss the relation between the Josephson-Transistor and the Superconducting Single Electron Transistor (SSET)[32]. The latter consists of two Josephson junctions separated by a superconducting grain, usually referred to as the *island*, which is capacitively (with capacitance $C_{\rm g}$) coupled to an external gate electrode. In a more figurative terminology we might call this device a SISIS junction. While the charging energy $E_{\rm C} = e^2/2C_\Sigma$ tends to fix the number of Cooper pairs on the island, the (conjugate) phase variable tends to be fixed by the Josephson coupling energy $E_{\rm J}$ of the two junctions. For the SSET, charging effects are dominant, $E_{\rm C} \gg E_{\rm J}$, and thus the total capacitance $C_\Sigma$ of the island must be small (but still[33] $C_{\rm g} \ll C_\Sigma$). Moreover we assume $E_{\rm C} < \Delta$ and hence the ground state of the island contains an even number of electrons at any gate voltage. Given this layout for the device, we expect the supercurrent to be suppressed by the 'Coulomb blockade' effect[34]. However, for specific values $V_{\rm g}^{\rm d}$ of the gate voltage the energies of two even charge states differing by $2e$ become degenerate. At these 'Coulomb resonances' the suppression of the Josephson current through the island is lifted and we find a large superflow. We can control the supercurrent by changing the gate voltage and hence the SSET constitutes a transistor device.

The above discussion shows that the SSET and the RJT are like devices, switching on as levels become degenerate; while for the SSET these levels belong to fixed charge states of the island, for the RJT these levels derive from transmission resonances. In both cases the degeneracy is lifted by the Josephson coupling $E\cos(\varphi/2)$, where the coupling constant $E$ is related to the transmission of the NIS boundaries, see below. Furthermore, the SSET and the RJT exhibit largely the same current-voltage characteristic close to these level degeneracies,

$$I = \frac{2e}{\hbar}\frac{E^2}{4e\gamma}\frac{\sin\varphi}{\sqrt{(V_{\rm g}-V_{\rm g}^{\rm d})^2 + \left(E\cos(\varphi/2)/e\gamma\right)^2}}, \qquad (15)$$

where the parameters $E$ and $\gamma$ have to be specified for each device. In fact, (15) yields the current through a symmetric SSET[33] if we substitute the energy parameter $E$ by the coupling energy $E_{\rm J}$ and the dimensionless constant $\gamma$ by the small ratio $C_{\rm g}/C_\Sigma$. Using the Ambegaokar-Baratoff relation[35] and the Landauer formula[36] we can reexpress the coupling energy in terms of more microscopic quantities: $E_{\rm J} = NT\Delta/4$, where $N \propto k_{\rm F}^2 A$ denotes the number of open channels in the tunnel junction, $A$ denotes its area, and $T$ its transmission coefficient. On the other hand, the RJT involves the parameters $E = \Gamma/2$ and $\gamma = \partial\mu_{x0}/\partial eV_{\rm g}$. Again, the resonance width is determined by geometrical quantities: $\Gamma \approx T\Lambda/\pi$, where $T$ is the transmittivity of the insulator layer in the triple barrier[37]. For flat inner barriers the quasi-classical method provides the simplification $\Lambda \sim 2(\mu_{x0}\varepsilon_{\rm L})^{1/2}$, with $\varepsilon_{\rm L} = \hbar^2\pi^2/2mL^2$. Note that, while charging effects dominate the physics of the SSET these are much less relevant for the RJT as the latter involves an 'open wire' rather than a 'closed island'; the adiabatic joints to the superconducting banks provide reservoirs which effectively screen the charge transport through the wire.

From Eq. (15) we can determine the critical supercurrent $I_{\rm c}$ as a function of the gate voltage near $V_{\rm g}^{\rm d}$. Apparently, $I_{\rm c}(V_{\rm g})$ defines a current peak of width $\delta V_{\rm g} = E/e\gamma$ that attains its maximum $I_{\max} = eE/\hbar$ at the degeneracy point. We estimate its slope by the ratio $I_{\max}/\delta V_{\rm g} = e^2\gamma/\hbar$ carrying the dimension of a conductance. For the SSET $\gamma \ll 1$ is determined through the small capacitance ratio $C_g/C_\Sigma$. The analogous quantity for the RJT is of order unity, implying that the RJT shows a more prominent slope: with $\partial\mu_{x0}/\partial eV_{\rm g} = \partial_d\mu_{x0}/\partial_{eV_{\rm g}}d$, and $\partial_d\mu_{x0} = 2(\varepsilon_{\rm F} - \mu_{x0})/d$ we have to determine the susceptibility of the channel width $d$ with respect to the gate voltage $V_g$. Making use of simple electrostatic considerations one easily finds that $\partial_{\mu_{x0}}d \sim a_{\rm B}/\varepsilon_{\rm F}$, where $a_{\rm B}$ denotes the Bohr radius in the semiconductor material[38,39]. Hence, $\gamma \sim a_{\rm B}/d$ and with $a_{\rm B}$ of order 10 nm typically we arrive at a value of order unity for the parameter $\gamma$.

Comparable energy scales $\Delta \sim \sqrt{\mu_{x0}\varepsilon_{\rm L}}$ can be reached in realistic short SINIS junctions ($L \lesssim \pi(\mu_{x0}/2m)^{1/2}\hbar/\Delta$). Furthermore, we can optimize the performance of the RJT by tuning the transparency of the insulating layers (the Dirac $\delta$-scatterers) until the resonance width $\Gamma$ approaches the resonance spacing $\Lambda$; such a choice of parameters produces still isolated current peaks of maximum height. On the other hand, the maximum superflow through the SSET scales with the number $N$ of open channels, $I_{\max} = eNT\Delta/4\hbar$, while the RJT as defined above is generically a single channel device with a critical supercurrent $I_{\max} = eT\sqrt{\mu_{x0}\varepsilon_{\rm L}}/\hbar\pi$; going over to a many channel RJT device, resonances from individual channels superpose at *different* values for the chemical potential and hence do not add up in general[40]. Also, a smoothing of the resonance structure has been observed in the numerical results by Wendin *et al.*[6]

Summarizing, superconducting transistors can be designed in terms of 'charge' (the SSET) or 'phase' devices (the JT). In the charge device, the island is separated from the superconducting leads through insulating barriers. On the other hand, switching channels in a perfect SNS junction one obtains a phase device with a (large) critical current $I_c = e/(\tau_0 + \hbar/\Delta)$ determined by the effective time $\tau_0 + \hbar/\Delta$ the charge needs to traverse the normal wire[13]. Such devices with perfect interfaces are difficult to fabricate — in reality we always have to account for a non-ideal transmission $T < 1$ through the SIN interfaces and we end up with a Fabry-Perot type resonator device. Sequential tunneling through the interface barriers then reduces the supercurrent by a factor $T^2$ in general. However, tuning the chemical potential to a scattering resonance the critical current of the junction remains large, $I_c \approx e\Gamma/2\hbar$ of order $T$ — again, the critical current is given by the time $\hbar/\Gamma$ the charge spends in the junction.

A second result we wish to emphasize here concerns the fact that the critical current is carried by the lowest quasi-particle level alone. This has been demonstrated for the SNS device in Ref. 13 and above for the SINIS junction for the case of strong resonances (deviations from the single level result are numerically (but not parametrically) larger away from weak resonances). The importance to know the dispersion of this level then provides a good *a posteriori* reason for studying the quasiparticle spectrum in such junctions. Corresponding spectroscopic experiments can be realized using multiprobe devices as proposed in the work of van Wees *et al.*[30]

We thank A. Golubov, V. Shumeiko, and G. Wendin for helpful discussions and the Swiss National Foundation for financial support. Work of N.M.C. and G.B.L. was partly supported by the Russian Foundation for Basic Research under contract number RFFI-000216617.

## APPENDIX: RESONANCE STRUCTURES IN ONE DIMENSION

We consider a one-dimensional potential landscape $V(x)$ confined to the interval $[-L/2, L/2]$. As a first example we concentrate on a symmetric barrier consisting of a broad ($m\Omega^2 = -\partial_x^2 V$, $\hbar\Omega \ll V(0)$) and smooth potential barrier, bounded by steps of height $V_S = V(L/2-0) - V(L/2+0)$ (see the inset of Fig. 8). Below we make use of the wave vectors $k_{sc} = \sqrt{2mE}/\hbar$ and $k_{nw} = \sqrt{2m(E-V_S)}/\hbar$ describing particles of energy $E$ in the wire close to the boundaries. The global transmission amplitude $t\exp(i\chi^t)$ is most easily obtained by determining the transfer-matrix[24] of the barrier between $-L/2-0$ and $L/2+0$ and we find the result

$$t\exp(i\chi^t) = \frac{t_i}{\cos(\chi^{t_i}) - i\kappa\sin(\chi^{t_i}) \pm i r_i\sigma}, \qquad \text{(A1)}$$

where $t_i\exp(i\chi^{t_i})$ and $r_i\exp(i\chi^{r_i})$ denote the transmission and reflection amplitudes of the inner smooth barrier. In (A1) we have introduced the definitions $\kappa = (k_{sc}/k_{nw} + k_{nw}/k_{sc})/2$ and $\sigma = (k_{sc}/k_{nw} - k_{nw}/k_{sc})/2$ containing the information about the steps. In our example, $\kappa$, $\sigma$, and $t_i$ show a weak dependence on energy and remain almost constant while $\exp(i\chi^{t_i})$ oscillates rapidly. The derivation of (A1) makes use of the relation $\chi^{r_i} - \chi^{t_i} = \pi/2 + \pi n$, $n \in \mathbf{Z}$, which follows from the unitarity of the scattering matrix; the term $\pm i r_i\sigma$ changes sign at each perfect resonance of $t_i$. Since the inner barrier was assumed to be smooth, we expect $t_i$ to exhibit no resonances at all and the term $r_i\sigma$ always carries a positive sign.

Next, we show that (A1) qualitatively reproduces the transmission amplitude shown in Fig. 2. We definine the function $z = 1/t\exp(i\chi^t)$, whose four arguments $\chi^{t_i}$, $\kappa$, $\sigma$, and $t_i$ depend on the energy. Since the inner scattering phase $\chi^{t_i}$ is the most energy sensitive argument we minimize $|z|$ with respect to $\chi^{t_i}$ (keeping $\kappa$, $\sigma$, and $t_i$ fixed at a given energy $E$). Thus we obtain the stationary phases $\chi^{t_i}_{\min}(E)$ belonging to the minima of $|z|$. Moreover, we can introduce the complex valued function $z_{\min}[E] = z[\chi^{t_i}_{\min}(E), \kappa(E), \sigma(E), t_i(E)]$, which is roughly constant when compared to $z[E]$. We can estimate the resonance energies by solving the equation $z[E_{res}] = z_{\min}[E_{res}]$ for $E_{res}$. Apparently, $z[E]$ describes an ellipse in the complex plane with half axes $1/t_i$ and $\kappa/t_i$. The center of this ellipse is shifted away from the origin by $ir_i\sigma/t_i$.

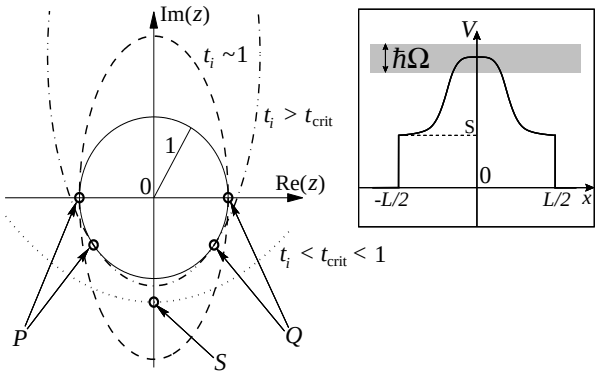


FIG. 8. Complex transmission amplitude through a smooth barrier bounded by steps. With decreasing energy $E$ the inverse $z = 1/t\exp(i\chi^t)$ moves counterclockwise on an ellipse, the center of which is positioned at $ir_i\sigma/t_i$ and shifts up the imaginary axis. As $t_i$ drops below $t_{crit}$ the perfect resonances at $P$ and $Q$ collapse at the bottom of the ellipse ($P \to S \leftarrow Q$) and transform into an imperfect (double) resonance.

Fig. 8 illustrates the behavior of $z_{\min}$ when $r_i$ grows from 0 to 1 in the intermediate region $E \in [V(0) - \hbar\Omega/2, V(0) + \hbar\Omega/2]$ (with a smooth inner barrier, $r_i$ is strictly monotonous, $r_i \approx 0$ for $E > V(0) + \hbar\Omega/2$ and

$r_i \approx 1$ for $E < V(0) - \hbar\Omega/2$). The distance from the origin to the bottom of the ellipse (point $S$) is always extremal. At high energies where $1 \approx t_i > 1/\kappa = t_{\rm crit}$, we observe *perfect* resonances: with $|z_{\rm min}| = 1$ these resonances are realized at the symmetric points $P$ and $Q$ where the ellipse touches the unit circle, see Fig. 8. As $t_i$ decreases the perfect resonances approach each other ($P$ and $Q$ move towards $S$) and merge with $S$ as $t_i \searrow t_{\rm crit}$. At energies $E \lesssim V(0)$ ($\Rightarrow t_i < t_{\rm crit}$) the reflection coefficient $r_i$ drops to zero, and $S$ becomes the closest point to the origin with $|z_{\rm min}| = (\kappa - \sigma r_i)/t_i > 1$; the resonances then have paired up and have become *imperfect*, with a height decaying rapidly with decreasing energy $E$.

Physically, this resonance structure originates from the interplay of two competing transparencies. The transmission probability through the potential steps is almost constant and much smaller than the transparency of the inner barrier for $E \gg V(0)$. In this regime the particles propagate freely and are reflected by the steps alone; thus we observe perfect resonances, and the shape of the smooth inner barrier only influences the resonance spacing. On the other hand, for $E \ll V(0)$ the inner barrier behaves like a hard wall while the steps are comparatively transparent. The global transmission through the barrier bounded by the steps is suppressed by the tunneling through the classically inaccessible region. The resonances of the subsystems consisting of a step and a potential hill account for the global imperfect resonances. Note that the barrier bounded by steps generates pronounced resonances only if $V_{\rm S} \gtrsim 0.7\, V(0)$.

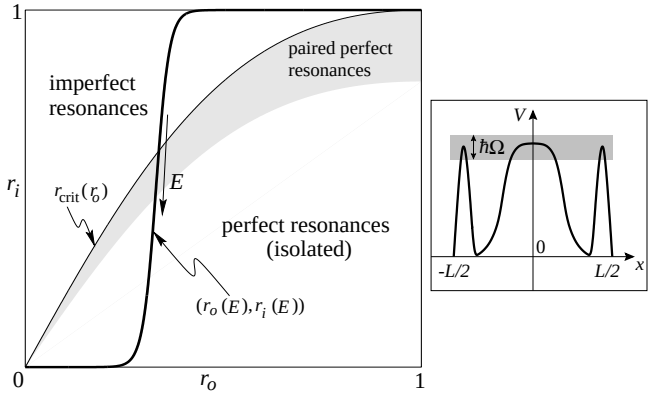


FIG. 9. The solid curve in the $(r_o, r_i)$ plane characterizes the energy dependence of the inner and the global reflection amplitudes in a symmetric triple barrier as shown in the inset. The domains of perfect and imperfect resonances are separated by the curve $r_{\rm crit}(r_o)$. In an narrow interval $\sim \hbar\Omega$ around $V(0)$ the reflection coefficent $r_i^2$ drops from 1 to 0; in this energy range $r_o$ can be considered as a constant.

In a second step we investigate the transmission amplitude through three arbitrary symmetric potential barriers, i.e., a triple barrier, see Fig. 9. The inner barrier is again smooth, whereas the two outer barriers (characterized by the transmission and reflection amplitudes $t_o \exp(i\chi^{t_o})$ and $r_o \exp(i\chi^{r_o})$) are assumed to be equal. Thus the global transmission amplitude takes the form

$$te^{i\chi^t} = \frac{t_i t_o^2 e^{i(\chi^{t_i} + 2\chi^{t_o})}}{1 + 2r_i r_o e^{i(\chi^{t_i} + \chi^{t_o})} - r_o^2 e^{i2(\chi^{t_i} + \chi^{t_o})}}. \qquad \text{(A2)}$$

In order to determine the resonance structure we evaluate the extrema of the modulus of the denominator in (A2) with respect to $\chi^{t_i} + \chi^{t_o}$ (we fix $t_i$ and $t_o$, which are less sensitive to changes in energy). A direct calculation yields the two extremal conditions $\cos(\chi^{t_i} + \chi^{t_o}) = -r_i(1 + r_o^2)/2r_o$ (I) and $\sin(\chi^{t_i} + \chi^{t_o}) = 0$ (II). Elementary manipulations show that the transmission amplitude exhibits *perfect* resonances in the first case. But condition I can only be satisfied as long as $r_i \le r_{\rm crit}(r_o) = 2r_o/(1 + r_o^2)$, i.e., for a reasonably transparent inner barrier (see Fig. 9). The extremal condition II requires a second distinction. Condition II(a) reads $\chi^{t_i} + \chi^{t_o} = 2\pi n$, $n \in \mathbf{Z}$. The critical points of this type always belong to local minima of $t$. Finally, we discuss condition II(b), $\chi^{t_i} + \chi^{t_o} = \pi + 2\pi n$, $n \in \mathbf{Z}$, which refers to local minima when $r_i < r_{\rm crit}$ and characterizes *imperfect* resonances in the regime $r_i > r_{\rm crit}$. Since the internal barrier was assumed to be smooth, the regime of perfect resonances lies at high energies $E > V(0) + \hbar\Omega/2$, where $r_i \approx 0$ and $r_o \gg r_i$. At low energies $E < V(0) - \hbar\Omega/2$, the resonances are always imperfect. Within the crossover region the perfect resonances attract each other pairwise and collapse to become imperfect as the energy decreases (see Fig. 2).

Other sources of resonances are discontinuities of the force $\partial_x V$ and effective mass steps. Technically they can be treated like Dirac $\delta$-scatterers and potential steps, respectively, as can be easily checked making use of the transfer-matrix formalism.


[1] For a review, see *Physics and Applications of Mesoscopic Josephson Junctions*, eds. H. Ohta and C. Ishii (The Physical Society of Japan, Kamiyama Printing, Tokyo, 1999).

[2] B.J. van Wees, H. van Houton, C.W.J. Beenakker, J.G. Williamson, L.P. Kouwenhoven, D. van der Marel, and C.T. Foxon, Phys. Rev. Lett. **60**, 848 (1988); D.A. Wharam, T.J. Thornton, R. Newbury, M. Pepper, H. Ahmed, J.E.F. Frost, D.G. Hasko, D.C. Peacock, D.A. Ritchie, and G.A.C. Jones, J. Phys. C **21**, L209 (1988).

[3] H. Takayanagi, T. Akazaki, and J. Nitta, Phys. Rev. Lett. **75**, 3533 (1995).

[4] H. van Houton, Appl. Phys. Lett. **58**, 1326 (1991).

[5] A. Chrestin, T. Matsuyama, and U. Merkt, Phys. Rev. B **49**, 498 (1994).

[6] G. Wendin and V.S. Shumeiko, Superlattices and Microstructures **20**, 569 (1996); G. Wendin and V.S. Shumeiko, P. Samuelsson, and H. Takayanagi, Jpn. J. Phys.

**38**, 354 (1999) and Superlattices and Microstructures **25**, 983 (1999).
[7] J.M. Krans, C.J. Muller, I.K. Yanson , Th.C.M. Govaert, R. Hesper, and J.M. van Ruitenbeek, Phys. Rev. B **48**, R14721 (1993).
[8] C.J. Muller, J.M. van Ruitenbeek, and L.J. de Jongh, Phys. Rev. Lett. **69**, 140 (1992).
[9] E. Scheer, N. Agrait, J.C. Cuevas, A.L. Yeyati, B. Ludoph, A. Martin-Rodero, G.R. Bollinger, J.M. van Ruitenbeek, and C. Urbina, Nature **394**, 154 (1998).
[10] L.I. Glazman, G.B. Lesovik, D.E. Khmel'nitskii, and R.I. Shekhter, Pis'ma Zh. Eksp. Theor. Fiz. **48**, 218 (1988) [JETP. Lett. **48**, 238 (1988)].
[11] C.W.J. Beenakker, Phys. Rev. Lett. **67**, 3836 (1991).
[12] A. Furusaki, H. Takayanagi, and M. Tsukada, Phys. Rev. Lett. **67**, 132 (1991) and Phys. Rev. B **45**, 10563 (1992).
[13] N.M. Chtchelkatchev, G.B. Lesovik, and G. Blatter, to appear in Phys. Rev. B (2000).
[14] T. Akazaki, H. Takayanagi, J. Nitta, and T. Enoki, Appl. Phys. Lett. **68**, 418 (1996).
[15] A.F. Morpurgo, T.M. Klapwijk, and B.J. van Wees, Appl. Phys. Lett. **72**, 966 (1998).
[16] Th. Schraepers, J. Malindretos, K. Neurohr, S. Lachenmann, A. van der Hart, G. Crecelius, H. Hardtdegen, and H. Lüth, Appl. Phys. Lett. **73**, 2348 (1998).
[17] J.J.A. Baselmans, A.F. Morpurgo, B.J. van Wees, and T.M. Klapwijk, Nature **397**, 43 (1999).
[18] A.Yu. Kasumov, R. Deblock, M. Kociak, B. Reulet, H. Bouchiat, I.I. Khodos, Yu.B. Gorbatov, V.T. Volkov, C. Journet, M. Burghard, Science **284**, 1508 (1999).
[19] L.I. Glazman and A.V. Khaetskii, J. Phys.: Condens. Matter **1**, 5005 (1989).
[20] P.F. Bagwell, Phys. Rev. B **46**, 12573 (1992).
[21] I.O. Kulik and A.N. Omel'yanchuk, Fiz. Nizk. Temp. **296** (1978) [Sov. J. Low Temp. Phys. **4**, 142 (1978)]; C. Ishii, Prog. Theor. Phys. **44**, 1525 (1970).
[22] A.F. Andreev, Sov. Phys. JETP **19**, 1228 (1964) [Zh. Eksp. Teor. Fiz. **46**, 1823 (1964)].
[23] G.A. Gogadze and A.M. Kosevich, Low Temp. Phys. **24**, 540 (1998) [Fiz. Nizk. Temp. **24**, 716 (1998)].
[24] B. Ricco and M.Ya. Azbel, Phys. Rev. B **29**, 1970 (1984).
[25] Note that in Ref. 13 basis states have been chosen where the phases vanish at the center of the junction.
[26] It is convenient to separate the effects of normal and Andreev scattering through a thin normal metallic layer of width $\delta \to 0$.
[27] Note that in our convention $\Gamma$ is twice as large as in Ref. 6.
[28] G. Wendin and V.S. Shumeiko, Phys. Rev. B **53**, R6006 (1996).
[29] V.S. Shumeiko, G. Wendin, and E.N. Bratus, Phys. Rev. B **48**, 13129 (1993).
[30] B.J. van Wees, K.-M.H. Lenssen, and C.J.P.M. Harmans, Phys. Rev. B **44**, 470 (1991).
[31] N.M. Chtchelkatchev *et al.*, unpublished.
[32] P. Joyez, P. Lafarge, A. Filipe, D. Esteve, and M.H. Devoret, Phys. Rev. Lett. **72**, 2458 (1994).
[33] M. Tinkham, *Introduction to Superconductivity* (McGraw-Hill, 1996).
[34] D.V. Averin and K.K. Likharev, in *Mesoscopic Phenomena in Solids*, edited by B.L. Altshuler, P.A. Lee, R.A. Webb (North-Holland, Amsterdam, 1991), p. 213.
[35] V. Ambegaokar and A. Baratoff, Phys. Rev. Lett. **10**, 486 (1963).
[36] M. Büttiker, Y. Imry, R.H. Landauer, and S. Pinhas, Phys. Rev. B **31**, 6207 (1985).
[37] The term 'triple barrier' is defined in Appendix A.
[38] L.I. Glazman and A.V. Khaetskii, Europhys. Lett. **9**, 263 (1989).
[39] I.A. Larkin and J.H. Davies, Phys. Rev. B **52**, R5535 (1995).
[40] N.M. Chtchelkatchev, Pis'ma Zh. Eksp. Theor. Fiz. **71**, 738 (2000).